DOI: 10.1002/(adma.201700411) **Article type: Communication**



Large Modulation of Charge Carrier Mobility in Doped Nanoporous Organic

Transistors

Fengjiao Zhang, Xiaojuan Dai, Weikun Zhu, Hyunjoong Chung, Ying Diao

anus

Dr. F. J. Zhang, H. Chung, W. K. Zhu and Prof. Y. Diao

Department of Chemical and Biomolecular Engineering, University of Illinois Urbana-

Champaign, 600 S. Mathews Ave., Urbana, IL 61801, USA

E-mail: yingdiao@illinois.edu

Xiaojuan Dai

Beijing National Laboratory for Molecular Sciences, Institute of Chemistry, Chinese

Academy of Sciences, Beijing 100190 (P.R. China)

Molecular doping of organic electronics has shown promise to sensitively modulate important device metrics. One critical challenge is the disruption of structure order upon doping of highly crystalline organic semiconductors, which significantly reduces the charge carrier mobility. We demonstrate a new method to achieve large modulation of charge carrier mobility via channel doping without

This is the author manuscript accepted for publication and has undergone full peer review but has not been through the copyediting, typesetting, pagination and proofreading process, which may lead to differences between this version and the <u>Version of Record</u>. Please cite this article as <u>doi:</u> 10.1002/adma.201700411.

This article is protected by copyright. All rights reserved.

disrupting the molecular ordering. Central to the method is the introduction of nanopores into the organic semiconductor thin films via a simple and robust templated meniscus-guided coating method. Using this method, we boost the charge carrier mobility of C_8 -BTBT transistors by almost sevenfold. We further demonstrate enhanced electron transport by close to an order of magnitude in a DPP-based donor-acceptor polymer. Combining spectroscopic measurements, DFT calculations and electrical characterizations, we identify the doping mechanism as partial-charge-transfer induced trap filling. The nanopores serve to enhance the dopant/OSC charge transfer reaction by exposing the π -electrons to the pore wall.

Keywords: morphology, organic field-effect transistor, doping, nanopore, solution coating

Doping has historically played a central role in modulating device performances of conventional inorganic semiconductors. Over the past few years, molecular doping has received increasing attention in the field of organic semiconductors (OSCs) for achieving high performance electronic and optoelectronic devices. [1-4] For organic transistors, doping has been applied to boost electrical conductivity and/or reduce contact resistance, when mobile charge carriers are introduced into the device via integer or partial charge transfer between the dopant and the OSC host. [1, 3, 5-9] Increased conductivity often comes at the expense of reduced on/off ratio detrimental to electronic switching. In many cases, however, dopant-induced charge carriers fill the trap states first, before mobile charge carriers can be generated. Doping by the trap filling mechanism is proven useful for tuning threshold voltage [10] amproving air stability [11-12], and enhancing charge carrier mobility [13-14] of the transistor devices without compromising the on/off ratio.

One of the major challenges in molecular doping lies in controlling the morphology of doped thin films, which is critical to maintaining high device performance.^[3, 8] Mixing of dopant in crystalline OSC matrix often disrupts the molecular packing to introduce structural and energetic disorders, thereby lowering charge carrier mobility.^[15-16] In addition, low dopant-OSC miscibility often results in large-scale phase separation and limits doping efficiency.^[14, 17-18] For these reasons, doping highly crystalline or semicrystalline transistor

devices is far more challenging than amorphous ones such as organic light-emitting diodes. ^[3] On the other hand, many recent high performance OSCs are based on highly crystalline small molecules, such as [1]Benzothieno[3,2-b]benzothiophene (BTBT)^[19] and dinaphtho-[2,3-b:2 ',3'-f]thieno[3,2-b]thiophene (DNTT)^[20] derivatives. Channel doping of these materials are rarely reported, and most studies focused on contact doping to facilitate charge injection instead. ^[5,21-22] One method to alleviate this issue is to deposit dopant as a separate layer on or beneath the OSC thin film, a.k.a. surface doping, or remote doping. However, surface doping cannot directly influence the buried conductive channel unless the film is very thin. ^[13, 23] A few other sequential deposition methods have also been demonstrated recently to prevent structural degradation during doping, such as solid-state diffusion via vapor deposition or solvent immersion. ^[8, 24] These methods have been successfully demonstrated for semicrystalline polymers; the dopant was found to reside in the solubilizing side chains without disrupting the backbone packing. However, it remains a challenge to effectively dope the conductive channels of highly crystalline devices.

In this work, we demonstrate a new method to significantly enhance the doping effect while maintaining the OSC structural integrity for both highly crystalline small molecules and semicrystalline polymers. The central concept of our approach is to introduce nanopores into the OSC layer using a simple and robust templated solution printing method prior to dopant deposition. Introducing nanopores effectively exposes the OSC conjugated core to the dopant, thereby enhancing their charge transfer reaction via co-facial stacking. The nanopores also grant dopant molecules direct access to the conductive channel of the transistor devices. We first demonstrate this method using a highly crystalline small molecule, 2,7-dioctyl[1]benzothieno[3,2-b][1]benzothiophene (C₈-BTBT), and a commonly employed p-dopant, 2,3,5,6-tetrafluoro-7,7,8,8,-tetracyanoquinodimethane (F₄-TCNQ). The

C₈-BTBT HOMO and the F₄-TCNQ LUMO can hybridize to form charge transfer complex, which was observed in their co-crystals.^[6] Surface doping of C₈-BTBT transistors by F₄-TCNQ has been reported before with the solvent immersion approach^[5], but only threshold voltage shift was observed via contact doping when the charge carrier mobility remained almost unchanged, indicating that channel doping was ineffective. This study again highlights the challenge of channel doping highly crystalline organic transistors. In this work, we show that our doping approach not only reduces the threshold voltage of C₈-BTBT transistors by over 20 V but also increases the charge carrier mobility by close to sevenfold upto 18.2 cm²V⁻¹s⁻¹ by decreasing the channel trap state density. We further demonstrate enhanced n-doping of an ambipolar conjugated polymer poly(diketopyrrolopyrrole-thiophene-thieno[3,2-b]thiophene-thiophene) (DPP2T-TT)^[26-27] using this approach.

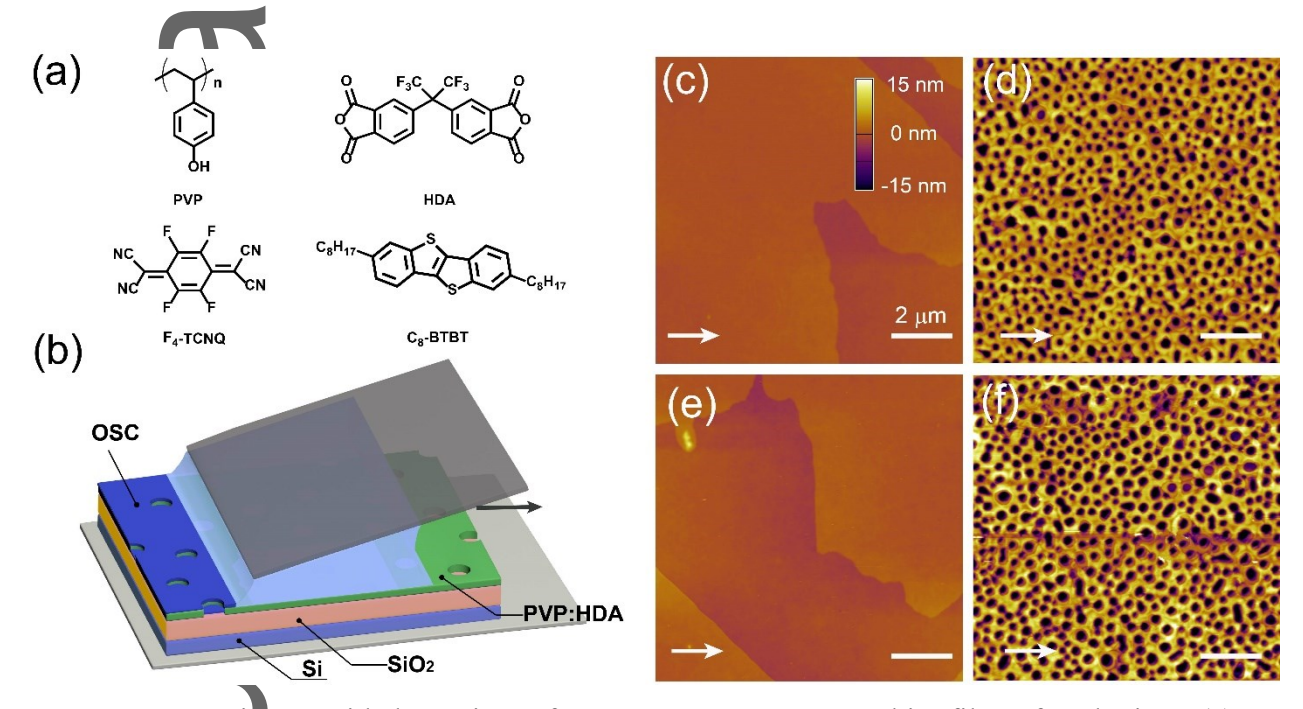


Figure 1. Meniscus-guided coating of nanoporous C_8 -BTBT thin films for doping. (a) Molecular structures of the porous template PVP:HDA, the dopant F_4 -TCNQ, and the OSC, C_8 -BTBT (b) Schematic of meniscus-guided coating on porous template. (c-f) AFM images of coated (c, e) nonporous and (d, f) porous C_8 -BTBT films (c, d) without (w/o) and (e, f) with (w/) F_4 -TCNQ. F_4 -TCNQ was deposited via spin-coating from 0.5 mg/mL water/acetone solution. The insert arrows indicate the coating direction. The scale bars in all images are 2 μ m.

The nanoporous C₈-BTBT thin film was prepared by a simple and additive meniscusguided solution coating method (Figure 1a,b). The key to the method is to direct the semiconductor deposition using a nanoporous insulating layer serving as the template, which can be fabricated over a large area via one-step microphase separation during spin coating. The simplicity and generality of this approach for fabricating nanoporous thin films stand in contrast to the conventional subtractive approaches based on lithography and etching, which involve complex procedures and corrosive chemicals.^[28-30] In brief, the porous template (Figure S1) was first fabricated by spin coating poly(4-vinylphenol) (PVP)/tetrahydrofuran (THF) solution with 4,4'-(hexafluoroisopropylidene)diphthalic anhydride (HDA) added as the cross-linking agent for PVP. [25] We recently showed that the addition of HDA decreases the miscibility of PVP with THF, thereby inducing microphase separation between a continuous PVP-rich phase and a discrete THF-rich phase. Subsequent THF evaporation leaves nanopores in the film. [25] The porous structure of the PVP:HDA template was then faithfully transferred to the C₈-BTBT thin film during one-step solution coating to form pores in the film. The typical film thickness and the pore depth are 20-30 nm. Doping was performed by spin-coating F₄-TCNQ from its water/acetone solution on the nanoporous C₈-BTBT thin film. We confirmed the formation and preservation of the C₈-BTBT nanoporous structures by tapping mode atomic force microscopy (AFM) before and after doping (Figure 1d, f, Figure S2 and Table S1), compared to nonporous thin films prepared using nonporous PVP:HDA templates (Figure 1c, e). It can be seen that the pore width and the pore depth hardly changed before and after C₈-BTBT deposition, across the entire range of pore sizes studied (Figure \$2 and Table S1). The thickness of the C₈-BTBT film is slight thinner than the depth of the pores, which indicates that the BTBT films inside the pores are not electrically connected with the rest of the films outside the pores. Interestingly, despite the significant change in mesoscale morphology, the introduction of nanopores and dopant deposition did not alter the macroscopic thin film morphology; close to millimeter-sized domains with well-defined terrace structures were obtained in all cases (Figure S3). We further performed grazing-incidence X-ray diffraction (GIXD) to characterize the thin film molecular packing (Figure S4 and S5). Not surprisingly, the F₄-TCNQ dopants didn't alter the C₈-BTBT molecular stacking, confirming that the surface doping process did not disrupt the host structure using our method. In addition, GIXD informs edge-on stacking of C₈-BTBT for all eases.

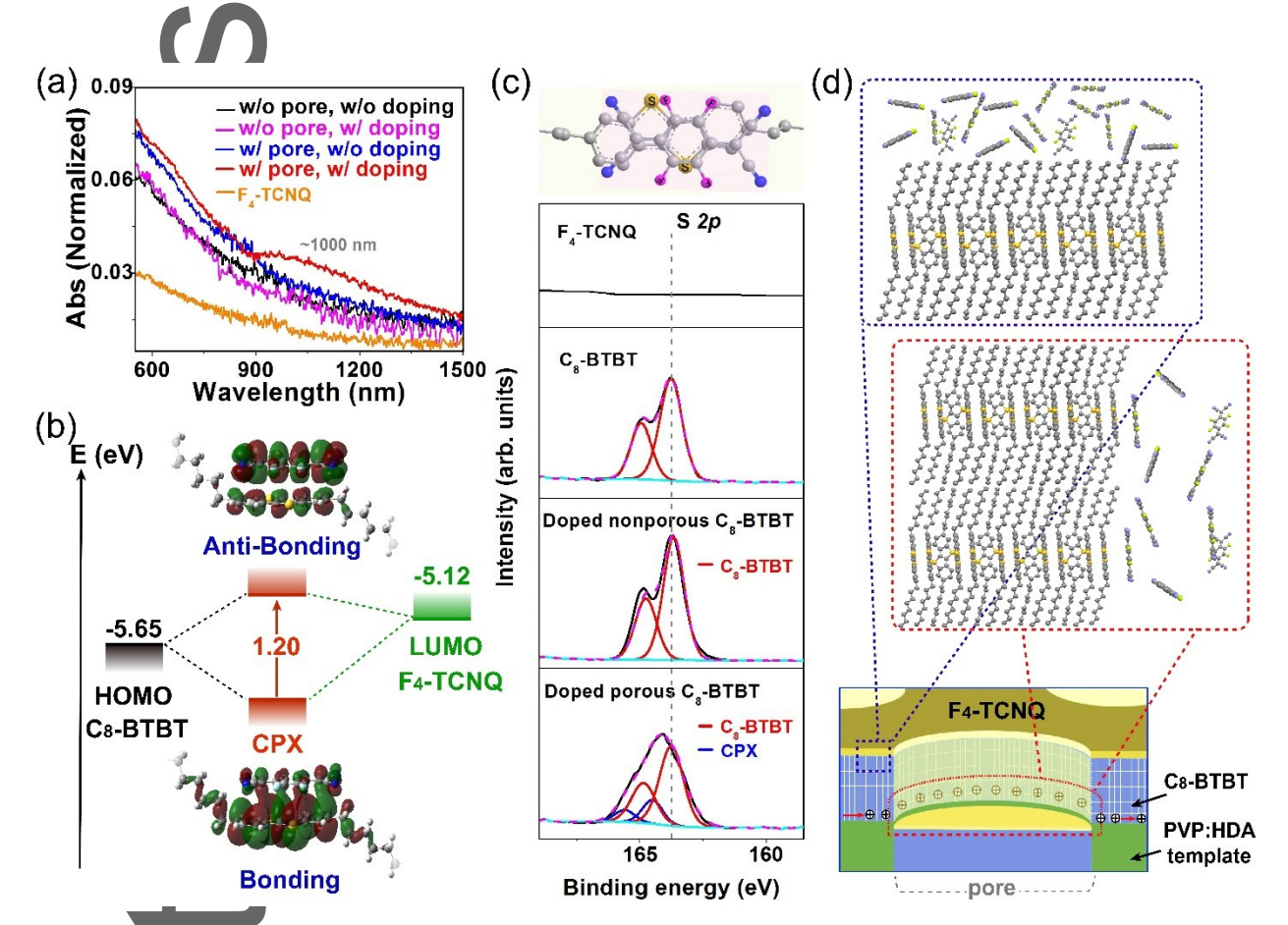


Figure 2. Analysis of doping mechanism in nanoporous devices. (a) UV-Vis-NIR absorption spectra of F₄-TCNQ film, nonporous and porous C₈-BTBT film before and after doping with F₄-TCNQ spin-coated from 0.5 mg/mL water/acetone solution. The average pore diameter is ~400 nm. (b) Energy level (E) diagram of C₈-BTBT, F₄-TCNQ and their charge transfer complex (CPX) with DFT-calculated orbital isosurface plots of the supramolecular hybrid orbitals. The corresponding energy levels were calculated using DFT for C₈-BTBT and F₄-TCNQ, and the optical band gap for CPX was calculated using TDDFT. (c) Deconvoluted S 2p XPS spectra of pristine and F₄-TCNQ doped (0.5 mg/mL) porous C₈-BTBT films as compared to doped nonporous ones. (d) Illustration of enhanced interactions between C₈-BTBT and F₄-TCNQ inside the nanopore (red) as compared to outside the nanopore (blue).

The enhanced interaction in the pore is attributed to co-facial stacking across the pore wall and direct access of dopant to the conductive channel.

To characterize the effectiveness of nanopores in facilitating dopant – OSC interactions, we first performed UV-Vis-NIR spectroscopy to analyze the electronic structures of F₄-TCNQ doped C₈-BTBT porous thin films (Figure 2a, Figure S6). The result was compared to several reference samples: neat F₄-TCNQ film, doped nonporous, pristine porous and pristine nonporous OSC thin films. Only in the case of doped porous thin films did we observe a new broad absorption band spanning from 870 to 1500 nm, peaked around 1000 nm (Figure 2a). From 250 to 870 nm, no new absorption features were observed in all cases (Figure S6 and Figure 2a). The new absorption band could be attributed to either F₄-TCNQ anion as a result of integer charge transfer, or C₈-BTBT/ F₄-TCNQ complex due to partial charge transfer, which are the two primary molecular doping mechanisms reported so far. [1] The F₄-TCNQ anions have been previously reported to exhibit sharp absorption peaks at around 767 nm and 869 nm. [7-8, 31] Given the absence of these absorption features in our case, we attribute the appearance of the broad absorption band to the formation of the C₈-BTBT/ F₄-TCNQ charge transfer complex (CPX). To validate this point, we further performed density functional theory (DFT) calculations and indeed obtained co-facially stacked CPX formed via frontier molecular orbital hybridization between the HOMO of C₈-BTBT and the LUMO of F₄-TCNQ (Figure 2b). Correspondingly, an optical gap of 1.20 eV appeared between a doubly occupied bonding and an unoccupied antibonding hybrid orbital calculated using timedependent density functional theory (TDDFT). Our simulation result is consistent with the previous report on C₈-BTBT/F₄-TCNQ co-crystals. [6] The calculated CPX optical gap closely matches with the experimentally observed absorption at ~1000 nm, which we assign to HOMO/LUMO transition of the CPX.

We further performed X-ray photoelectron spectroscopy (XPS) measurements to reveal the atomic-level details of OSC-dopant interactions in the CPX. From the geometrically optimized CPX structure obtained from DFT (Figure 2b,c), we inferred that the chemical environment of the sulfur atoms in the C₈-BTBT thiophene units and that of the fluorine atoms in Fa-TCNQ may be sensitively modulated by the CPX formation. Figure 2c shows the high-resolution scans of the S 2p XPS spectra. In pristine C₈-BTBT, a double-peak was observed with peak binding energies at 164.9 and 163.8 eV, corresponding to S $2p_{1/2}$ and S $2p_{3/2}$ respectively [32] Upon doping with F₄-TCNQ, a noticeable shift in the peak binding energies as well as a change in the spectra shape was observed for the porous films. Peak deconvolution revealed the emergence of a new doublet with peak binding energies at 165.6 and 164.5 eV respectively, which we assigned to S $2p_{1/2}$ and S $2p_{3/2}$ in the CPX. The 0.7 eV increase in the binding energy indicates that the sulfur atoms in C₈-BTBT are partially oxidized (deficient in electron density) in the CPX. At the same time, we observed a ~0.2 eV decrease in the F1s binding energy in doped samples, indicating that the fluorine atoms in F₄-TCNQ is partially reduced in the CPX (Figure S7a). This observation corroborates the simulated CPX structure by DFT. In contrast to porous samples, the shape and peak positions of S 2p spectra for nonporous films hardly changed upon doping, and peak deconvolution uncovered negligible CPX S 2p peaks correspondingly (Figure 2c). This result, together with the UV-Vis-NIR study (Figure 2a), provides strong evidence that the presence of nanopores in C₈-BTBT substantially enhanced its interaction with F₄-TCNQ as to enable the formation of their CPX.

Combining the spectroscopy with morphology characterizations, we propose a morphology model of doped porous thin films to elucidate the mechanism of nanopore-induced CPX formation (Figure 2d). For C₈-BTBT films without pores, the post-deposited

The doni

F₄-TCNQ molecules reside on the top surface of the film; dopant diffusion into the film is unlikely given the dense molecular packing of highly crystalline C₈-BTBT. Further considering edge-on stacking in the C₈-BTBT thin film (Figure S4), F₄-TCNQ mainly 'see' the densely packed alkyl chains, while the conjugated cores are buried underneath. In this case, CPX cannot form unless a small amount of F₄-TCNQ molecules find their way into the grain boundaries. In the case of the nanoporous thin film, F₄-TCNQ molecules deposited on the pore wall can interact with the exposed conjugated cores of C₈-BTBT to form CPX. In addition, the dopant has direct access to the originally buried conductive channel, further enhancing the doping effect for transistor devices.

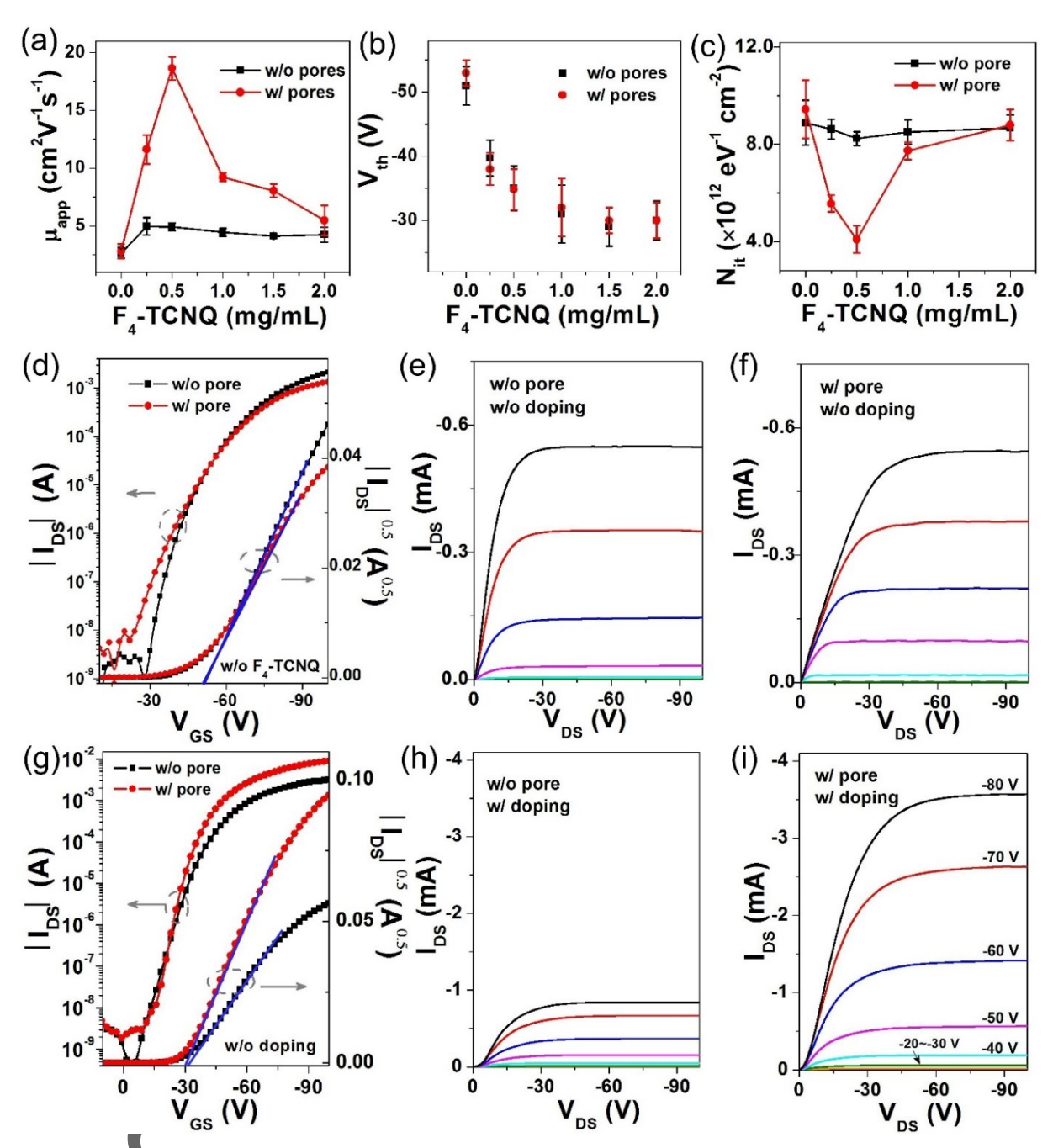


Figure 3. C_8 -BTBT field-effect transistor device characteristics comparing porous vs. nonporous, doped vs. pristine devices. (a) Apparent mobility in the saturation regime, (b) threshold voltage and (c) interfacial trap state density as a function of F_4 -TCNQ solution concentration used for spin coating. (d, g) Transfer and (e, f, h, i) output curves of C_8 -BTBT OFET (d, e, f) spin-coated with water/acetone solvent and (g, h, i) doped with F_4 -TCNQ spin-coated from 0.5 mg/mL water/acetone solution. The channel length and width are 70 and 4500 μ m, respectively. Transfer curves were measured with V_{DS} = -100V. For porous C_8 -BTBT devices, the channel width was corrected by accounting for the film porosity, which is 0.375±0.005 obtained from image analysis. The apparent mobility was calculated as the slope of the blue line shown in (d) and (g). Gate voltage dependent mobilities are shown in Figure S11.

To evaluate the effect of doping on transistor device performance, we fabricated topcontact, bottom-gate organic field-effect transistors (OFET). Ag source-drain electrodes (35 nm) were thermally evaporated onto the printed C₈-BTBT thin film to define a channel length and width of 70 µm and 4500 µm, respectively. We also tried Au for electrodes, but found significant damage to the film during thermal evaporation, possibly due to higher deposition temperature of Au than Ag. We first measured the device in the pristine state, and the same device was measured again after surface doping so as to eliminate the effect of sample-tosample variation. Doping was performed by spin coating F₄-TCNQ solution of 0 to 2.0 mg/mL on the Ca-BTBT transistor devices. The doped devices were stored under vacuum overnight to remove residual solvent. Figure 3a compares the doping effect on porous vs. nonporous devices at various dopant concentrations. For porous devices, the apparent charge carrier mobility in the saturation regime remained the same as nonporous devices for both pristing devices and for those spin-coated with neat solvent (Table S2 and Figure S8). Note that introducing nanopores slightly decreased the on-current (Figure 3d and Figure S8a) due to reduced effective channel width. After channel width correction accounting for film porosity (see experimental section in SI), the extracted charge carrier mobility was found unaffected by the presence of nanopores of 400 nm. This result validates that our method of printing nanoporous thin films preserves the molecular packing and charge percolation pathways, and therefore does not compromise the charge transport properties when the pore sizes are small. We note that we indeed observed a decrease of charge carrier mobility when pore sizes exceed 400 nm (Figure S9 and Table S3), which can be attributed to increased film discontinuity (Figure S10) or higher defect/trap density in the OSC film as the pore size increases (Table S3). Nonetheless, a significant enhancement was obtained for doped porous compared to pristine porous OFETs across the entire range of pore sizes investigated

(0~850nm). Below, we focus on discussing results obtained at the optimal pore size of 400 nm shown in Figure 3.

With increasing dopant solution concentration from 0 to 0.5 mg/ml, the average apparent mobility of nanoporous devices increased by close to sevenfold from 2.8 to 18.2 cm²V⁻¹s⁻¹, while the apparent mobility of the nonporous devices only increased moderately from 2.7 to 4.9 cm²V s⁻¹ (Table S2). Further increasing dopant solution concentration decreased the mobility for both porous and nonporous devices. Figures 3g-i compare the representative saturation regime transfer and output curves of porous and nonporous devices at 0.5 mg/ml dopant concentration. Introducing nanopores significantly improved the device on-current while keeping the on/off ratio high at 10⁶. We note that the apparent mobilities calculated within the range of gate voltage specified in Figures 3d-g may not represent the intrinsic mobilities due to gate-voltage-dependent contact resistance and other non-idealities. [33-35] Nonetheless, the gate-voltage-dependent mobilities of doped porous devices remained significantly higher than nonporous ones across the entire range of the gate voltage measured (Figure S11). In addition to enhanced mobility, we also observed reduced threshold voltage from -50 V to -30 V with the increase of dopant solution concentration for both porous and nonporous devices (Figure 3b). These results show that introducing nanopores markedly enhanced the channel doping effect, possibly by the mechanism of charge trap filling from OSC-dopant partial charge transfer. [2, 7, 36-37] Previously work showed that two distinct doping regimes exist: trap-filling and dopant saturation/reserve. [2, 36] When the number density of dopant is below that of charge traps, doping is under the trap-filling regime, which we believe is the case of this study.

To understand whether the observed mobility enhancement is indeed a result of channel charge-trap filling, we calculated the interfacial trap state density (N_{it}) from the subthreshold

swing following the equation $N_{it} = C_{ox}(S \times e/(k_BT \ln 10)-1)/e^2$, where e is the elementary charge, S is the subthreshold swing, k_B is the Boltzmann constant, C_{ox} represents the capacitance per unit area of the dielectric layer and T is the absolute temperature. For nonporous devices, N_{it} decreased only slightly from $8.9 \times 10^{12} \text{ eV}^{-1} \text{ cm}^{-2}$ to $8.2 \times 10^{12} \text{ eV}^{-1} \text{ cm}^{-2}$ with increasing dopant solution concentration (Figure 3c). In contrast to nonporous devices, N_{it} of nanoporous devices reduced by more than twofold from $9.4 \times 10^{12} \text{ eV}^{-1} \text{ cm}^{-2}$ in pristine devices to $4.1 \times 10^{12} \text{ eV}^{-1} \text{ cm}^{-2}$ at the dopant concentration of 0.5 mg/mL. Remarkably, the dependence of interfacial trap density on dopant concentration is highly consistent with that of the mobility for both porous and nonporous devices (Figure 3a), which strongly supports our hypothesis that the doping-induced mobility enhancement is a result of nanopore-enabled interfacial trap filling.

To validate the proposed mechanism of nanopore-induced channel doping as opposed to contact doping, we intentionally applied contact doping at the Ag/C₈-BTBT interface with MoO₃. As expected, porous devices did not exhibit improved mobility than nonporous ones with contact doping alone (Figure S12a). When the devices were further spun-coated with F₄-TCNQ, we again observed pronounced mobility enhancement from 2 to over 6 cm²V⁻¹s⁻¹ for porous devices, whereas the mobility hardly changed in the nonporous case (Figures S12a, S13). Furthermore, the doping-concentration-dependent mobility and the threshold voltage (Figures S12) both exhibited the same trends as those without MoO₃ contact doping (Figure 3a, b). All results consistently point to the same nanopore-enhanced doping mechanism as channel doping by interfacial trap filling, as opposed to contact doping.

Below, we hypothesize the mechanism of trap filling in the conductive channel via CPX formation, illustrated in Figure 4. The C_8 -BTBT/ F_4 -TCNQ charge-transfer complexes, once formed on the pore wall, replace F_4 -TCNQ to serve as the actual dopants. [2, 7] As the F_4 -

TCNQ concentration increases, CPX forms on the pore wall to increase dopant concentration. With the decrease of Fermi level (E_F), more CPXs become ionized (negatively charged). The holes thus generated fill the traps in the circumjacent C₈-BTBT films leading to increased mobility we observed. Further increasing the F₄-TCNQ concentration consumes more C₈-BTBT molecules during CPX formation, thereby reducing the effective channel width to result in decrease of mobility. The two competing effects lead to an optimum doping level.

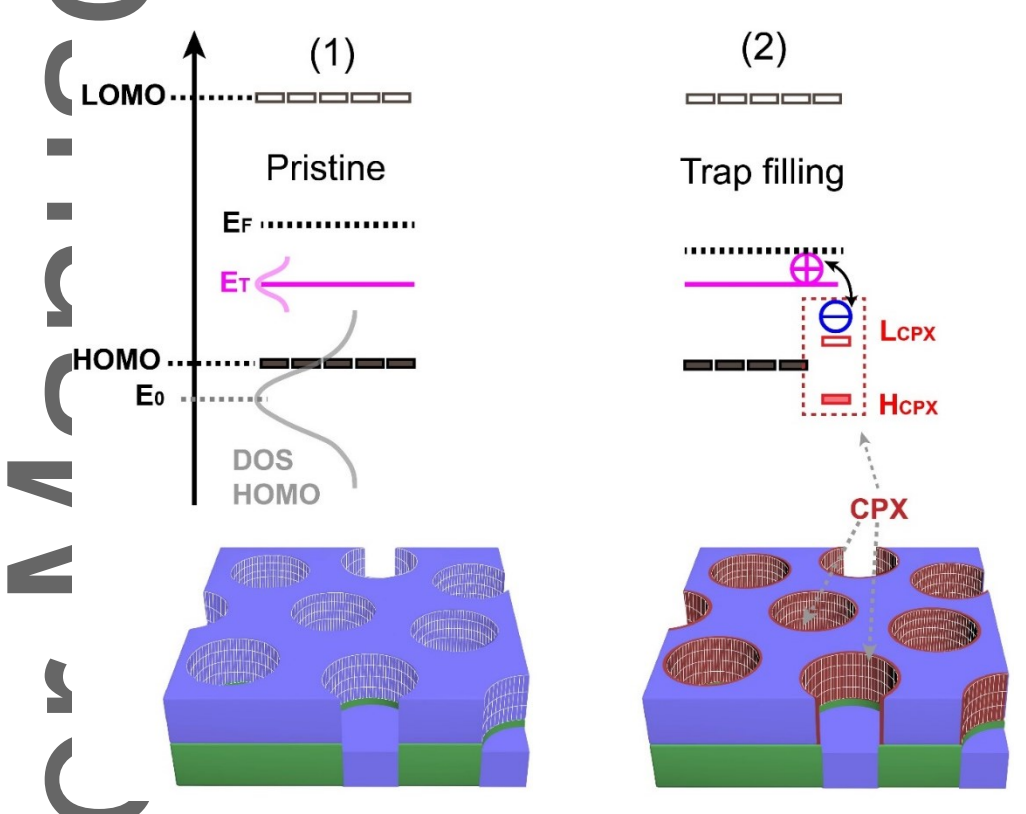


Figure 4. Hypothesized mechanism of CPX induced trap-filling in porous OSC films. (1) Energy level diagram for pristine porous C_8 -BTBT film before doping. E_{HOMO} , E_{LUMO} and E_F are the HOMO, LUMO and Fermi energy level. E_T denotes the energy level of deep trap states. (2) Charge transfer complex (CPX) formation at the pore wall upon doping. Ionization of CPX creates holes to fill the trap states. L_{CPX} and H_{CPX} denote the unoccupied antibonding and doubly occupied bonding hybrid orbitals of CPX respectively. The F_4 -TCNQ layer on the top of the OSC film is omitted for clarity, due to minimal CPX formation.

To demonstrate the generality of our approach, we further fabricated nanoporous conjugated polymers for enhancing n-channel doping of ambipolar transistor devices. So far, there have been few reports on n-channel doping of OFETs.^[11, 14] Naab and Bao et al. reported n-doping of 6,13-bis(triisopropylsilylethynyl)pentacene (TIPS-pentacene) by

solution shearing its blend with dopant 2-(2-methoxyphenyl)-1,3-dimethyl-2,3-dihydro-1Hbenzoimidazol-3-ium (o-MeO-DMBI-I).^[14] Although the dopant was found to be largely phase separated from TIPS-pentacene, the authors attributed the effective doping to dopant deposition at the grain boundaries which passivated the electron traps. In this work, we demonstrate nanopore-enhanced n-doping of an ambipolar polymer DPP2T-TT doped by polyethyleneimine (PEI) (Figure S14a). PEI has been successfully applied as an effective ntype dopant to convert ambipolar and p-type polymers to n-type polymers or to increase conductivity of p-type polymers, for both field-effect transistors and photovoltaic devices. [40] Using the templated meniscus-guided coating method described earlier, we prepared nanoporous DPP2T-TT thin films templated by PVP:HDA (Figure S14b,c). The details of OFET device fabrication are summarized in the supporting information. The pristine DPP2T-TT devices exhibited predominant p-channel behavior, with hole mobility up to 0.32 cm²V⁻¹s⁻ ¹, on/off ratio higher than 10⁵, and threshold voltage of -28 V (Figure S15 and S16a-b). We note that no direct comparison of device performance can be made with previous reports on high performance DPP2T-TT OFETs due to the difference in side chain structures. [26] Negligible n-channel performance was observed in these undoped devices possibility due to presence of electron traps (oxygen, water) in the as fabricated films. Surface doping with PEI at sufficiently high dopant concentration has significantly enhanced n-channel characteristics while passivated p-channel behavior (Figure S15, Figure S16c-d). Remarkably, the highest electron mobility achieved for doped porous OFETs is almost one order of magnitude higher than the one without pores (Figure S15). Regarding the doping mechanism, we speculate that the lone-pair electrons of the nitrogen atoms in PEI lead to hole trapping/electron trap filling. 400.cl On the other hand, the reported electronic structure of PEI contradicts previous and our results.^[41] The actual n-doping mechanism by PEI remains unclear and requires further investigations. Nonetheless, this result indicates that our method of doping

nanoporous thin films can be broadly applicable for tuning transistor device characteristics including, but not limited to, charge carrier mobility and p/n channel behavior.

In conclusion, we have demonstrated a new method to achieve large modulation of charge carrier mobility via channel doping without disrupting the molecular ordering and thin film morphology. Central to the method is the introduction of nanopores into the OSC thin films via a simple and robust templated meniscus-guided coating method, and subsequent solution deposition of a dopant layer atop the porous OSC film. Using this method, we successfully doped highly crystalline C₈-BTBT thin films with F₄-TCNQ of low concentrations. The apparent hole mobility of C₈-BTBT increased by almost sevenfold to 18.2 cm²V⁻¹s⁻¹, and the threshold voltage decreased by over 20 V, without compromising the high on/off ratio of 10⁶. In contrast, the mobility of nonporous C₈-BTBT hardly increased upon doping while the threshold voltage dropped by the same extent. We attributed the mobility enhancement to trap filling in the conductive channel, and showed that indeed, the interfacial trap state density decreased by more than twofold in doped porous devices while almost unchanged in nonporous ones. We further analyzed the doping mechanism in depth combining UV-Vis-NIR and XPS spectroscopy with DFT calculations. These studies revealed that doping of porous OSC led to the formation of charge-transfer complex (CPX) involving co-facially stacked C₈-BTBT and F₄-TCNQ. Without nanopores, the CPX formation was negligible. We attributed the nanopore-induced CPX formation to enhanced co-facial interactions between the OSC and the dopant across the pore wall near the conductive channel. Our method is not only applicable to highly crystalline small molecule OSCs, but also to semicrystalline conjugated polymers. We demonstrated close to an order of magnitude enhancement in electron mobility of PEI doped DPP2T-TT transistors when nanopores were introduced. We expect our method to significantly advance the field of molecular doping by enhancing the

doping effect without causing structural and energetic disorders. Our approach is of broad impact given its potential applicability to a wide range of systems and the importance of doping in numerous device applications.

Supporting Information

Supporting Information is available from the Wiley Online Library or from the author.

Acknowledgements

This research was financially supported by the startup funds of University of Illinois. The authors gratefully acknowledge senior research scientist Richard T. Haasch for help with the XPS measurements. Part of this work was conducted at the Frederick Seitz Materials Research Laboratory Central Facilities, University of Illinois at Urbana-Champaign, and at Advanced Photon Source, Argonne National Laboratory.

Received: ((will be filled in by the editorial staff))
Revised: ((will be filled in by the editorial staff))
Published online: ((will be filled in by the editorial staff))

- [1] I. Salzmann, G. Heimel, M. Oehzelt, S. Winkler, N. Koch, Acc. Chem. Res. 2016, 49, 370.
- [2] M. L. Tietze, P. Pahner, K. Schmidt, K. Leo, B. Lüssem, *Adv. Funct. Mater.* **2015**, *25*, 2701.
- [3] B. Lussem, C. M. Keum, D. Kasemann, B. Naab, Z. Bao, K. Leo, *Chem. Rev.* **2016**, *116*, 13714.
- [4] B. Lüssem, M. Riede, K. Leo, *Phys. Status Solidi (A)* **2013**, *210*, 9.

- [5] J. Soeda, Y. Hirose, M. Yamagishi, A. Nakao, T. Uemura, K. Nakayama, M. Uno, Y. Nakazawa, K. Takimiya, J. Takeya, *Adv. Mater.* **2011**, *23*, 3309.
- [6] H. Mendez, G. Heimel, A. Opitz, K. Sauer, P. Barkowski, M. Oehzelt, J. Soeda, T. Okamoto, J. Takeya, J. B. Arlin, J. Y. Balandier, Y. Geerts, N. Koch, I. Salzmann, *Angew. Chem. Int. Ed. Engl.* **2013**, *52*, 7751.
- [7] H. Mendez, G. Heimel, S. Winkler, J. Frisch, A. Opitz, K. Sauer, B. Wegner, M. Oehzelt, C. Rothel, S. Duhm, D. Tobbens, N. Koch, I. Salzmann, *Nat. Commun.* **2015**, *6*, 8560.
- [8] K. Kang, S. Watanabe, K. Broch, A. Sepe, A. Brown, I. Nasrallah, M. Nikolka, Z. Fei, M. Heeney, D. Matsumoto, K. Marumoto, H. Tanaka, S. Kuroda, H. Sirringhaus, *Nat. Mater.* **2016**, *15*, 896.
- [9] Y. Gao, A. L. Yip, K. S. Chen, K. M. O'Malley, O. Acton, Y. Sun, G. Ting, H. Chen,A. K. Jen, *Adv. Mater.* 2011, 23, 1903.
- [10] B. H. Lee, G. C. Bazan, A. J. Heeger, Adv. Mater. 2016, 28, 57.
- [11] P. Wei, J. H. Oh, G. Dong, Z. Bao, J. Am. Chem. Soc. 2010, 132, 8852.
- [12] M.J. Ford, M. Wang, H. Phan, T. Q. Nguyen, G. C. Bazan, *Adv. Funct. Mater.* **2016**, 26, 4472.
- [13] J. H. Kim, S. W. Yun, B. K. An, Y. D. Han, S. J. Yoon, J. Joo, S. Y. Park, *Adv. Mater.* **2013**, *25*, 719.
- [14] B. D. Naab, S. Himmelberger, Y. Diao, K. Vandewal, P. Wei, B. Lussem, A. Salleo,Z. Bao, Adv. Mater. 2013, 25, 4663.
- [15] J. Gao, J. D. Roehling, Y. Li, H. Guo, A. J. Moulé, J. K. Grey, *J. Mater. Chem. C* **2013**, *1*, 5638.
- [16] H. Kleemann, C. Schuenemann, A. A. Zakhidov, M. Riede, B. Lüssem, K. Leo, *Org. Electron.* **2012**, *13*, 58.

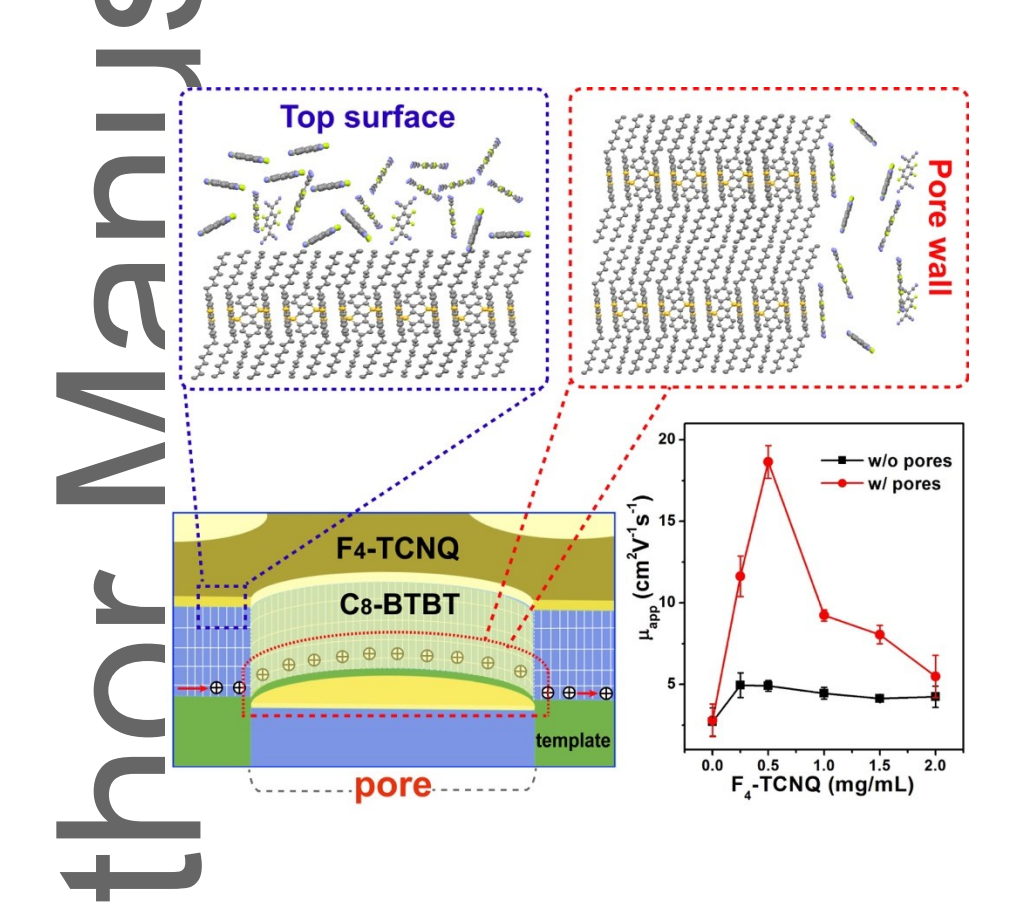
- [17] D. T. Duong, H. Phan, D. Hanifi, P. S. Jo, T. Q. Nguyen, A. Salleo, *Adv. Mater.* 2014, 26, 6069.
- [18] R. A. Schlitz, F. G. Brunetti, A. M. Glaudell, P. L. Miller, M. A. Brady, C. J. Takacs,C. J. Hawker, M. L. Chabinye, *Adv. Mater.* 2014, 26, 2825.
- [19] H. Ebata, T. Izawa, E. Miyazaki, K. Takimiya, M. Ikeda, H. Kuwabara, T. Yui, *J. Am. Chem. Soc.* **2007**, *129*, 15732.
- [20] K. Nakayama, Y. Hirose, J. Soeda, M. Yoshizumi, T. Uemura, M. Uno, W. Li, M. J. Kang, M. Yamagishi, Y. Okada, E. Miyazaki, Y. Nakazawa, A. Nakao, K. Takimiya, J. Takeya, *Adv. Mater.* **2011**, *23*, 1626.
- [21] T. Minari, P. Darmawan, C. Liu, Y. Li, Y. Xu, K. Tsukagoshi, *Appl. Phys. Lett.* **2012**, *100*, 093303.
- [22] F. Ante, D. Kalblein, U. Zschieschang, T. W. Canzler, A. Werner, K. Takimiya, M. Ikeda, T. Sekitani, T. Someya, H. Klauk, *Small* **2011**, *7*, 1186.
- [23] T. Hählen, C. Vanoni, C. Wäckerlin, T. A. Jung, S. Tsujino, *Appl. Phys. Lett.* **2012**, *101*, 033305.
- [24] S. N. Patel, A. M. Glaudell, D. Kiefer, M. L. Chabinyc, ACS Macro Lett. 2016, 5, 268.
- [25] F. J. Zhang, Q. Ge, M. Erfan, J. G. Mei, D. Ying, Adv. Funct. Mater. 2017, Accepted.
- [26] J. Li, Y. Zhao, H. S. Tan, Y. L. Guo, C. A. Di, G. Yu, Y. Q. Liu, M. Lin, S. H. Lim, Y. H. Zhou, H. B. Su, B. S. Ong, Sci. Rep. 2012, 2, 754.
- [27] Z. Chen, M. J. Lee, R. Shahid Ashraf, Y. Gu, S. Albert-Seifried, M. Meedom Nielsen,
 B. Schroeder, T. D. Anthopoulos, M. Heeney, I. McCulloch, H. Sirringhaus, *Adv. Mater.*2012, 24, 647.
- [28] R. G. H. Lammertink, M. A. Hempenius, J. E. van den Enk, V. Z. H. Chan, E. L. Thomas, G. J. Vancso, *Adv. Mater.* **2000**, *12*, 98.

- [29] A. J. Storm, J. H. Chen, X. S. Ling, H. W. Zandbergen, C. Dekker, *Nat. Mater.* **2003**, 2, 537.
- [30] J. K. Yu. S. Mitrovic, D. Tham, J. Varghese, J. R. Heath, *Nat. Nanotechnol.* **2010**, *5*, 718.
- [31] L. Ma, P. Hu, H. Jiang, C. Kloc, H. Sun, C. Soci, A. A. Voityuk, M. E. Michel-Beyerle, G. G. Gurzadyan, *Sci. Rep.* **2016**, *6*, 28510.
- [32] L. Lyu, D. Niu, H. Xie, N. Cao, H. Zhang, Y. Zhang, P. Liu, Y. Gao, *J. Chem. Phys.* **2016**, *144*, 034701.
- [33] E. G. Bittle, J. I. Basham, T. N. Jackson, O. D. Jurchescu, D. J. Gundlach, *Nat. Commun.* **2016**, 7, 10908.
- [34] T. Demura, C. Rolin, T. H. Ke, P. Fesenko, J. Genoe, P. Heremans, J. Takeya, *Adv. Mater.* 2016, 28, 151.
- [35] L. McCulloch, A. Salleo, M. Chabinyc, *Science* **2016**, *352*, 1521.
- [36] M. L. Tietze, K. Leo, B. Lüssem, Org. Electron. 2013, 14, 2348.
- [37] I. Salzmann, G. Heimel, S. Duhm, M. Oehzelt, P. Pingel, B. M. George, A. Schnegg,K. Lips, R. P. Blum, A. Vollmer, N. Koch, *Phys. Rev. Lett.* 2012, *108*, 035502.
- [38] M. R. Niazi, R. Li, E. Qiang Li, A. R. Kirmani, M. Abdelsamie, Q. Wang, W. Pan, M. M. Payne, J. E. Anthony, D. M. Smilgies, S. T. Thoroddsen, E. P. Giannelis, A. Amassian, *Nat. Commun.* **2015**, *6*, 8598.
- [39] W. L. Kalb, B. Batlogg, Phys. Rev. B 2010, 81, 035327.
- [40] [a] M. Shim, A. Javey, N. W. Shi Kam, H. Dai, J. Am. Chem. Soc. 2001, 123, 11512.
- [b] B. Sun, W. Hong, E. S. Thibau, H. Aziz, Z. H. Lu, Y. Li, ACS Appl. Mater. Interfaces
- 2015, 7, 18662. [c] W. Huang, L. Zeng, X. Yu, P. Guo, B. Wang, Q. Ma, R. P. H. Chang, J.
- Yu, M. J. Bedzyk, T. J. Marks, A. Facchetti, Adv. Funct. Mater. 2016, 26, 6179. [d] J. Wang,
- L. Xu, B. Zhang, Y.-J. Lee, J. W. P. Hsu, Adv. Electron. Mater. 2017, 3, 1600458.

[41] Y. Zhou, C. Fuentes-Hernandez, J. Shim, J. Meyer, A. J. Giordano, H. Li, P. Winget, T. Papadopoulos, H. Cheun, J. Kim, M. Fenoll, A. Dindar, W. Haske, E. Najafabadi, T. M. Khan, H. Sojoudi, S. Barlow, S. Graham, J. L. Bredas, S. R. Marder, A. Kahn, B. Kippelen, *Science* 2012, 336, 327.

Large Modulation of Charge Carrier Mobility in Doped Nanoporous Organic Transistors

Fengjiao Zhang, Xiaojuan Dai, Weikun Zhu, Hyunjoong Chung, Ying Diao



Doping of organic electronics without disrupting molecular packing is a critical challenge preventing effective modulation of charge transport properties. We report on enhanced charge-transfer doping in crystalline small molecule and polymer transistors by introducing nanopores in organic semiconductors via meniscus-guided coating. Nanopores led to

dramatic increase in charge carrier mobility by promoting charge transfer reaction across the pore wall.